ACS APPLIED MATERIALS & INTERFACES

Research Article

www.acsami.org

A Novel and Functional Single-Layer Sheet of ZnSe

Jia Zhou,*[,†] Bobby G. Sumpter,[†,‡] Paul R. C. Kent,[†,‡] and Jingsong Huang[†,‡]

[†]Center for Nanophase Materials Sciences, Oak Ridge National Laboratory, Bethel Valley Road, Oak Ridge, Tennessee 37831-6493, United States

[‡]Computer Science and Mathematics Division, Oak Ridge National Laboratory, Bethel Valley Road, Oak Ridge, Tennessee 37831-6367, United States

Supporting Information

ABSTRACT: The recently synthesized freestanding four-atom-thick double-layer sheet of ZnSe holds great promise as an ultraflexible and transparent photoelectrode material for solar water splitting. In this work, we report theoretical studies on a novel three-atom-thick single-layer sheet of ZnSe that demonstrates a strong quantum confinement effect by exhibiting a large enhancement of the band gap (2.0 eV) relative to the zinc blende (ZB) bulk phase. Theoretical optical absorbance shows that the largest absorption of this ultrathin single-layer sheet of ZnSe occurs at a wavelength similar to its four-atom-thick double-layer counterpart, suggesting a comparable behavior on incident photon-to-current conversion efficiency for solar water splitting, among a wealth of potential applications. The results presented herein for ZnSe may be generalized to other group II-VI analogues.

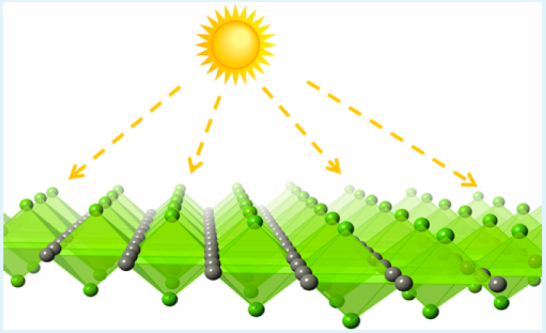

KEYWORDS: *Two-dimensional materials, DFT, GW approximation, BSE, photovoltaic*

INTRODUCTION

Novel two-dimensional (2D) colloidal nanocrystals of semiconducting binary II-VI cadmium or zinc chalcogenides ZnX and CdX (X = S, Se, or Te) of different thicknesses are attracting significant interest due to their intrinsic tunability and potential suitability for a broad range of applications.[1−6] These 2D nanocrystals demonstrate a dimensional reduction distinct from other low dimensional materials such as 0D quantum dots and 1D quantum wires,[7,8] and typically display thickness-dependent absorption and emission spectra.[1,2,9] In addition to these 2D colloidal nanosheets coated by organic ligands, clean and freestanding 2D sheets of ZnX and CdX, inspired by graphene and its diverse inorganic analogues,[10−14] have also stepped into the limelight.[2,15−18] For example, Xie and co-workers fabricated a freestanding four-atom-thick sheet of ZnSe, possessing a clean surface and a honeycomb lattice.[2] Their photoelectrochemical test for solar water splitting exhibits a photocurrent density 4−10 times higher than that of ligand-coated layers, 8 times higher than quantum dots, and nearly 200 times higher than that of its 3D bulk.[2] This breakthrough benefited from pioneering work on various 2D lamellar inorganic−organic hybrid structures $[M_mX_m(L)_n]$ (where M is metal, X is chalcogenide, and L is alkylamine ligand) synthesized by solvothermal and soft colloidal template techniques in the past decade.[4,9,19,20] Specifically, the lamellar hybrid structures can be exfoliated by sonication in appropriate solvents into 2D colloidal nanosheets,[4] from which freestanding 2D sheets can be then made by removing the ligands with heat.[2] Synthesis of the four-atom-thick honeycomb sheet of ZnSe thus suggests a route for the synthesis of other freestanding 2D sheets of ZnX and CdX in various thicknesses by using 2D colloidal nanosheets or lamellar hybrid structures as precursors. More recently, several theoretical studies proposed freestanding single- to few-layer sheets of ZnX and CdX with honeycomb lattices as potential synthesis targets.[15−18] In this work, we report theoretical studies on a three-atom-thick single-layer sheet of ZnSe that is stabilized by its unusual square lattice configuration. This ultrathin sheet displays a quantum confinement effect stronger than the experimentally synthesized four-atom-thick sheet of ZnSe.

COMPUTATIONAL METHOD

All first-principles calculations were carried out using the Vienna ab initio simulation package (VASP)[21−24] unless otherwise stated. In density functional theory (DFT) calculations, the Kohn−Sham equations were solved using the projector-augmented wave (PAW) method.[25,26] The Perdew−Burke−Ernzerhof (PBE) functional[27,28] and PAW potentials were employed. First, we searched for new configurations by fifteen independent molecular dynamics (MD) simulations at 500 K each lasting for 20 ps starting from a 2 × 2 supercell as constructed from the X-ray structure of the zinc blende phase of ZnSe.[29] This was followed by a full structural relaxation of the new configurations of interest employing the PBE functional in combination with the long-range dispersion correction implemented by Grimme.[30] Finally, a 1 × 1 primitive cell of the optimized geometry was subjected to electronic structure and optical property calculations

Received: August 21, 2014
Accepted: December 22, 2014
Published: December 23, 2014

DOI: 10.1021/am505655m
ACS Appl. Mater. Interfaces 2015, 7, 1458−1464

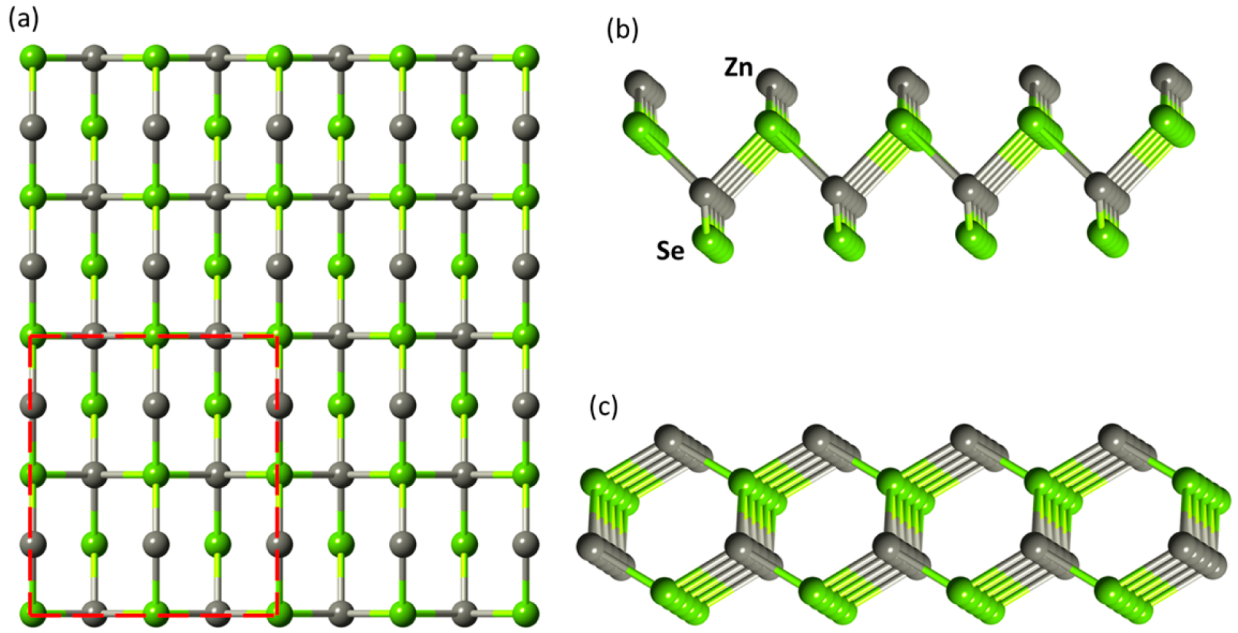

Figure 1. Search for new configurations of ultrathin ZnSe starts with a 2 × 2 supercell containing a four-atom layer of ZnSe excised in the (100) plane from the X-ray structure of its ZB bulk phase: top view (a) and two side views (b, c). The red dashed lines indicate the periodic boundary condition.

using DFT, random-phase approximation (RPA), and many-body perturbation theories including quasiparticle G_0W_0 and Bethe–Salpeter equation (BSE).[31,32] The results of the three-atom-thick single-layer sheet were compared with those of the experimentally synthesized, four-atom-thick, double-layer sheet of ZnSe. To verify the stability of the discovered new structure, phonon calculations were carried out within a local density approximation using the density functional perturbation theory (DFPT) in Quantum Espresso.[33] For all calculations on layered sheets, the vacuum separation was set to 20 Å to ensure the periodic images are well separated and do not interact. Further computational details are given in the Supporting Information.

RESULTS AND DISCUSSION

We began our search for the novel single-layer sheet of ZnSe by scrutinizing its face indexing in the ZB bulk phase. The experimentally realized four-atom-thick honeycomb sheet of ZnSe corresponds to the (110) cleavage of its 3D bulk in the ZB phase,[2] hereafter denoted as ZB110. In contrast, the ultrathin three-atom-thick sheet corresponds to the (100) cleavage in the ZB phase, which is denoted as ZB100. The main difference between the two scenarios is the presence or absence of a honeycomb lattice. According to the calculations by Xie and co-workers, ZB100 has much higher surface energy than ZB110 (0.122 eV/Å vs 0.035 eV/Å).[2] Despite the absence of a honeycomb lattice, Ithurria et al. successfully synthesized 2D colloidal nanoplatelets of CdX with 4 to 11 monolayers in the ZB100 orientation, which may have been stabilized by the surface ligands.[1] Herein we constructed the thinnest ZB100 sheet of ZnSe by excising a four-atom layer in the (100) plane from the X-ray structure of its bulk ZB phase. Figure 1 shows a 2 × 2 supercell of the ZB100 four-atom layer containing two layers of Zn and two layers of Se. Following the terminology in ref 1, this ZB100 sheet consists of two monolayers. A one-monolayer ZB100 sheet is out of the question because it consists of unbonded rows of atoms. By ab initio MD simulations, we found that under mild temperature, this four-atom layer can be converted to a stable ultrathin configuration consisting of a square lattice of alternating Zn and Se atoms. It is due to the square lattice configuration that this material is stabilized despite its ZB100 orientation. With its structure fully relaxed, the electronic, phonon, and optical properties of the novel ZnSe sheet are calculated by DFT and state-of-the-art many-body perturbation theory including quasiparticle *GW* approach and BSE. Note that the calculations are performed for only ZnSe in order to compare with the experimentally realized four-atom-thick honeycomb sheet of ZnSe but the conclusions may be generalized to other II-VI analogues.

First, we examine the ab initio MD simulation results for the 2 × 2 supercell. As can be seen in Figure 2, the potential

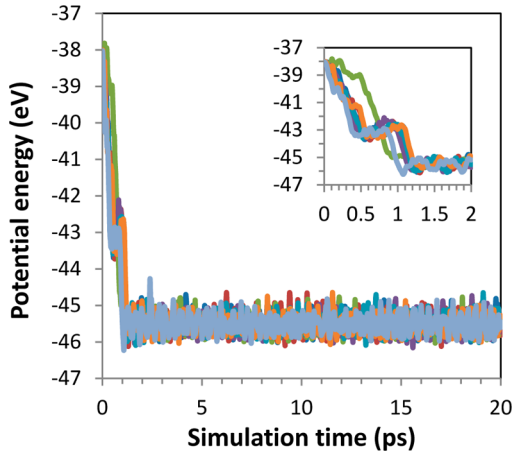

Figure 2. Seven out of fifteen independent ab initio MD simulations display two plateaus (the inset shows a zoomed in view of the high-energy plateau). Visualizations of the trajectories reveal that the high-energy plateau are due to formation of a Zn–Zn dimer on one surface and a Se–Se dimer on the other surface, whereas the low-energy plateau corresponds to the formation of a square lattice of alternating Zn and Se atoms. Other observations and byproducts obtained from additional MD simulations are discussed in the Supporting Information.

DOI: 10.1021/am505655m
ACS Appl. Mater. Interfaces 2015, 7, 1458–1464

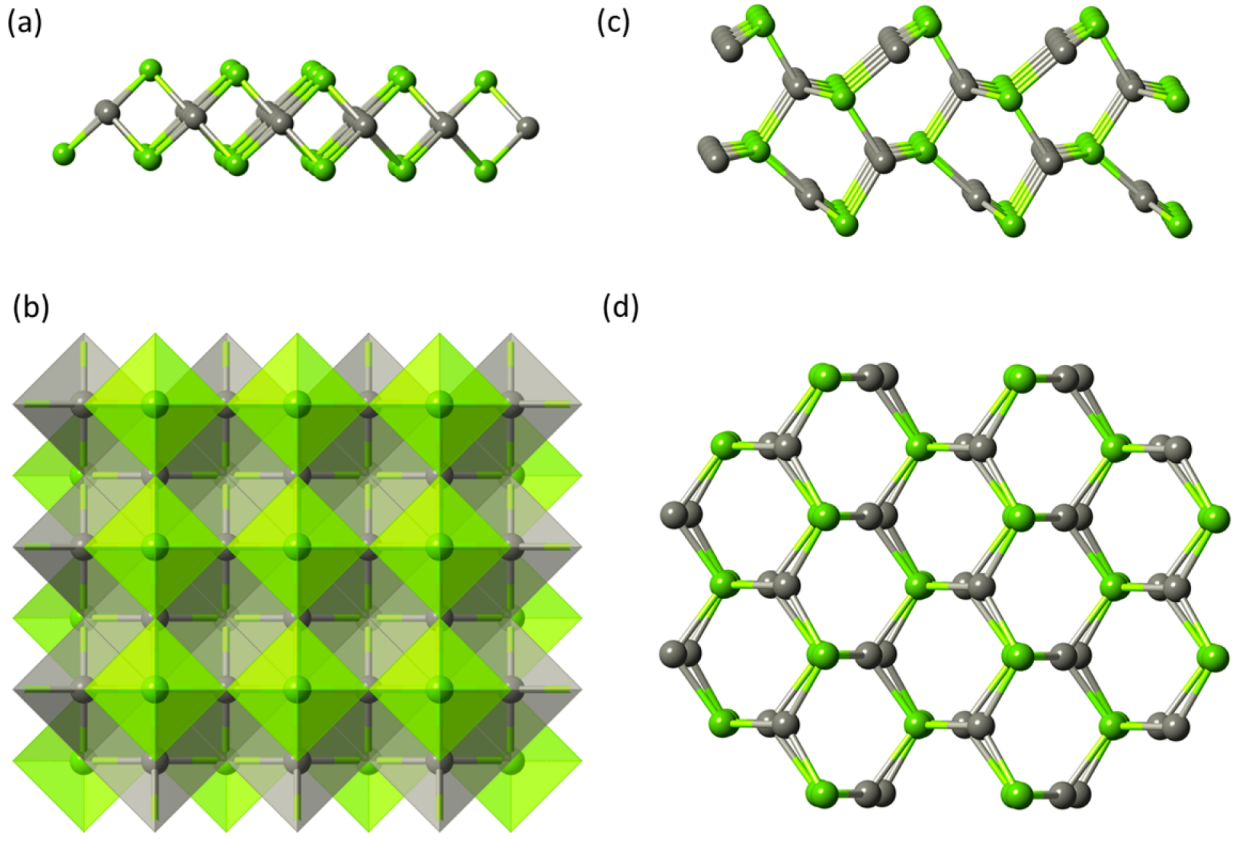

Figure 3. Side view (a) and top view (b) of the fully relaxed ultrathin three-atom-thick ZnSe sheet. The Zn-centered tetrahedrons and the Se-apexed pyramidals are shown in gray and green, respectively. Side view (c) and top view (d) of the four-atom-thick ZnSe sheet from ref 2, which is also fully relaxed for property calculations.

energies in seven out of fifteen trajectories clearly display two plateaus. Note that the MD results presented do not have spin polarization, because spin-polarized MD simulations with ferromagnetic and antiferromagnetic spin configurations led to the same observations (Figure S1, Supporting Information). Visualizations of the trajectories reveal that the high-energy plateau at ca. −43 eV, lasting from 0.5 to 1 ps, can be ascribed to the formation of a Zn−Zn dimer on the top surface and a Se−Se dimer on the bottom surface. Note that the dimerizations were observed for the 2 × 2 supercell while a primitive cell does not allow such a process to take place. It is found that the surface reorganization is essential for the formation of new configurations. On the other hand, the low-energy plateau at −45.5 eV corresponds to the formation of a square lattice of alternating Zn and Se atoms. Analysis of the trajectories indicates that the Zn−Zn and Se−Se dimers dissociate immediately after the top-layer Zn atoms move below the first layer of Se atoms, resulting in a three-atom-thick layer with a square lattice. An MD snapshot at 20 ps is shown in Figure S2 (Supporting Information), while its relaxed structure is shown in Figure 3. The square lattice resembles a single layer of atoms removed from the bulk rocksalt structure of ZnSe but with a strong corrugation. In light of the high pressure of ca. 13 GPa that is needed for the bulk rocksalt to become the ground state structure,[34,35] the discovery of such a rocksalt-like single-layer sheet at ambient pressure is unexpected. As will be clear from the phonon calculation (described below), this rocksalt-like single-layer sheet is a dynamically stable structure. The three-atom-thick layer with the square lattice found by the MD simulations is then fully relaxed for subsequent electronic and optical property calculations. Lattice vectors and Cartesian coordinates are tabulated in Table S1 (Supporting Information).

In addition to the above-mentioned seven trajectories, five additional trajectories only show the high-energy plateau at ca. −43 eV, which last from 0.5 to 20 ps (Figure S3, Supporting Information). Because this plateau corresponds to the formation of Zn−Zn and Se−Se dimers, the square lattice shown in Figures S1 and 3a,b (Supporting Information) was not observed within the 20 ps simulations. In three more simulations, low-energy plateaus from −44.5 to −45.5 eV were indeed observed (Figure S4, Supporting Information); however, these plateaus correspond to other configurations that are different from the square lattice. It turns out that one trajectory led to a double-layer sheet each consisting of fused 4- and 8-membered rings (Figure S5, Supporting Information), another yielded a double-layer sheet each consisting of honeycomb lattices, equivalent to fused 6- and 6-membered rings (Figure S6, Supporting Information), whereas the third simply gave a hybrid of the former two scenarios (Figure S7, Supporting Information). The plateau energy of the double-layer sheet with fused 4- and 8-membered rings is higher at −44.5 eV, whereas that of the double-layer sheet with honeycomb lattice is comparable to the square lattice at −45.5 eV (Figure S4, Supporting Information). Consequently, the plateau energy of the hybrid scenario is between that of the fused 4-/8-membered rings and that of the honeycomb lattice.

Next we turn to the relaxed structure of the freestanding single-layer sheet of ZnSe (Figure 3a,b). As can be seen from the side view, the ultrathin single-layer sheet of ZnSe is three

DOI: 10.1021/am505655m
ACS Appl. Mater. Interfaces 2015, 7, 1458−1464

atoms thick, with Zn atoms sandwiched in the middle by two layers of Se atoms located on the outsides, giving a thickness of merely 3.0 Å (Table 1). Also, from the side view, the single-layer ZnSe resembles typical transition-metal dichalcogenides (TMDs), such as MoS_2 or WSe_2, but with a different one-to-one atomic ratio. In fact, the coordination of single-layer ZnSe is rather different from that of TMDs. As can be seen from the top view, each Zn/Se atom is tetrahedrally coordinated with its neighboring Se/Zn atoms, giving a pseudotetragonal lattice. Specifically, each Zn atom is located at the center of the tetrahedron formed by its four neighboring Se atoms, whereas each Se atom is located at the apex of the square pyramid formed by the Se atom and its four Zn neighbors. This geometry is quite different from the experimentally synthesized four-atom-thick ZnSe sheet,[2] which is characterized by a honeycomb lattice (Figure 3c,d). In fact, the four-atom-thick ZB110 ZnSe sheet consists of two corrugated honeycomb sheets stacked in an AA fashion, giving a double-layer structure and a thickness of 6.5 Å (Table 1). With the van der Waals (vdW) radius of the surface Se atoms considered, the actual thickness of the double-layer structure is about 1 nm, in reasonable agreement with the experimental 0.9 nm found by atomic force microscopy (AFM). It is thus expected that the AFM thickness of the single-layer sheet of ZnSe should be at most 6.8 Å.

Table 1. Thickness, Total Energy (E_{tot}), and Band Gap (E_g) of the Zinc Blend Bulk Phase, ZB110 Double-Layer Sheet, and ZB100 Single-Layer Sheet

properties	bulk	ZB110 double-layer sheet	ZB100 single-layer sheet
thickness (Å)[a]		6.5, (10.3, 9.1[b])	3.0, (6.8)
E_{tot} (eV)[c]	−6.634	−6.318	−6.133
E_g (eV)[d]	1.12/2.25	1.91/3.37	2.14/4.21

[a]Numbers inside the parentheses have the vdW radius of Se atom considered (1.9 Å). [b]Experimental thickness found by atomic force microscopy (AFM) (ref 2). [c]Energy per formula unit of ZnSe. [d]Band gaps by PBE/G_0W_0.

As can be also seen from Table 1, the energy per formula unit is −6.318 and −6.133 eV for the ZB110 double-layer sheet and the novel ZB100 single-layer sheet, respectively, both of which are higher than that for the ground-state bulk phase of zinc blende at −6.634 eV. Obviously, both of the layered sheets are metastable structures, similar to the theoretically predicted layered sheets of CdX (X = S, Se, and Te).[16] However, we note that having a relatively higher energy does not preclude the possibility for the layered sheets to be synthesized, given its dynamic stability as will be seen from the phonon calculations shown below and the experimental synthesis demonstrated for ZB110 double-layer sheet. This can be true, especially considering that the single-layer sheet may be further stabilized by the vdW interactions with appropriate substrates. For example, Tusche et al. and Weirum et al. have shown that the deposition of thin layers of zinc oxide on the top of a metal substrate leads to the formation of a honeycomb single-layer structure, which is stabilized by dispersion interactions.[36,37]

For the properties of the single-layer ZnSe, we first studied its phonons, bands, and density of states (DOS). As can be seen in Figure 4a, no imaginary frequencies are observed in its phonon dispersions (and phonon DOS, not shown), confirming the dynamical stability of the single-layer ZnSe. This behavior is similar to that of the experimentally synthesized four-atom-thick sheet.[2,16] Figure 4b shows its band structure, which displays a direct band gap at the Γ point, the same as the bulk ZnSe.[38] Figure 4c shows the total DOS

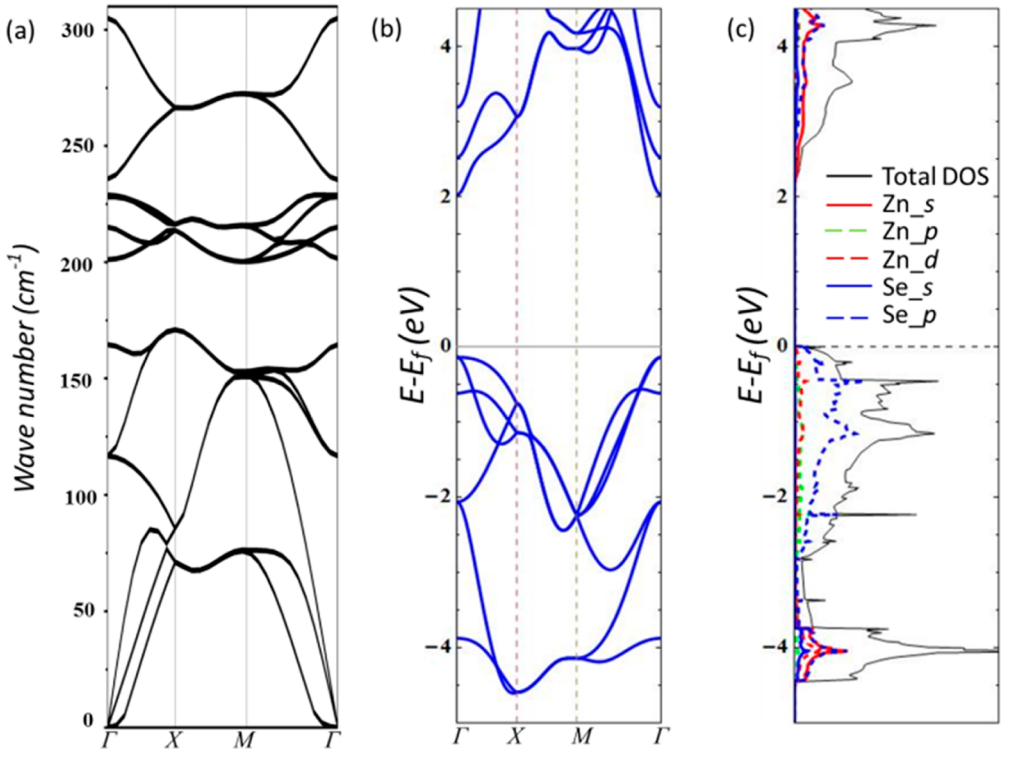

Figure 4. Dispersion of phonon modes (a), band structure (b), and total/partial DOS (c) of the ultrathin single-layer sheet of ZnSe.

DOI: 10.1021/am505655m
ACS Appl. Mater. Interfaces 2015, 7, 1458−1464

and the partial DOS projected onto the *s*, *p*, and *d* states of Zn and Se atoms. It can be seen that the valence bands from −2 to 0 eV are dominated mainly by Se's *p* states. On the other hand, the conduction bands from 2 to 4 eV consist mainly of the hybridization from Zn's *s* and Se's *p* states. The presence of Zn's *s* states in the conduction bands indicates charge transfer from Zn to Se, leading to an ionic character in this seemingly covalent compound as implied from its tetrahedrally coordinated structure. However, with the presence of Se's *p* states in the conduction bands, it appears that the charge transfer is incomplete. Bader charges calculated for Zn and Se atoms amount to $q = \pm 0.72$, respectively. This substantial magnitude implies a large degree of ionic character. However, the single-layer sheet has slightly lower Bader charges than its bulk ZB phase with a magnitude of $q = \pm 0.75$, showing that the single-layer sheet has a slightly higher degree of covalent character than its bulk structure. The coexistence of both ionic and covalent characters is well accepted for II-VI compounds.[39] A rigorous quantification of the ionicity and covalency will require more thorough studies.

From the band structure and the DOS, the band gap for the single-layer ZnSe sheet is 2.14 eV at the DFT level. Because it is well-known that the PBE functional usually underestimates the band gaps,[40] we also performed quasiparticle G_0W_0 calculations, which significantly increased the band gap to 4.21 eV (Table 1). In comparison, the band gap for the double-layer ZB110 sheet is 1.91 and 3.37 eV by PBE and G_0W_0, respectively. As a further comparison, the theoretical band gap of the ZB bulk phase of ZnSe is found to be 2.25 eV according to our G_0W_0 calculation (Table 1), which is significantly improved from the DFT result of 1.12 eV with respect to the experimental band gap of ca. 2.7 eV.[41] Relative to the bulk, both 2D sheets display an enhancement of the band gap. However, the enhancement in the ultrathin ZB100 single-layer ZnSe is significantly larger than that in the ZB110 double-layer ZnSe (2.0 vs 1.1 eV), indicating a stronger quantum confinement effect in the former. The stronger quantum confinement effect may be ascribed to the fact that the thickness of the novel ultrathin single-layer ZnSe (3.0 Å) is less than half of that of the experimental synthesized ZB110 double-layer ZnSe (6.5 Å). While revising this paper, we were made aware of the recent progress on PAW potentials containing norm-conserving partial waves that may give rise to finite-basis-set correction for quasiparticle energies.[42] These new norm-conserving PAW potentials for Zn and Se were tested for the bulk, giving 2.57 eV (similar to the 2.55 eV obtained in ref 42), which is a 0.3 eV increase over the previous PAW potentials. Due to the increased valence electron count and higher plane wave cutoff energies required by these new potentials, as well as the higher atom count and vacuum spacing required, we were not able to apply them to the single-layer sheets due to computational costs. We expect the general trends predicted in this study to be robust, but future application of the new potentials may yield slightly increased band gaps. On the basis of the quasiparticle band gap with self-energy corrections, next we employ the BSE equation to address optical absorption spectrum.

We address the optical property of the single-layer ZnSe sheet in terms of optical absorbance $A(\omega)$, which is defined as the fraction of photons of energy $E = \hbar\omega$ absorbed by the single-layer sheet. For in-plane (of the single-layer sheet) polarized light, $A(\omega)$ is calculated by $A(\omega) = \omega \times L \times \varepsilon_2/c$, where ω is the frequency of photon, L is the interlayer spacing between the isolated ZnSe layers, ε_2 is the imaginary part of the dielectric function, and c is the speed of light in vacuum.[43] The imaginary part of the dielectric function is calculated by solving RPA and BSE. The level of theory adopted for the optical property calculations is first applied to the ZB phase of the bulk ZnSe for the validation of theory, and the absorption spectra computed from both RPA and BSE are in excellent agreement with the experimentally measured absorption spectrum (Figure S8, Supporting Information).

Figure 5 shows the calculated optical absorbance $A(\omega)$ as a function of the photon frequency ω for both the novel ultrathin

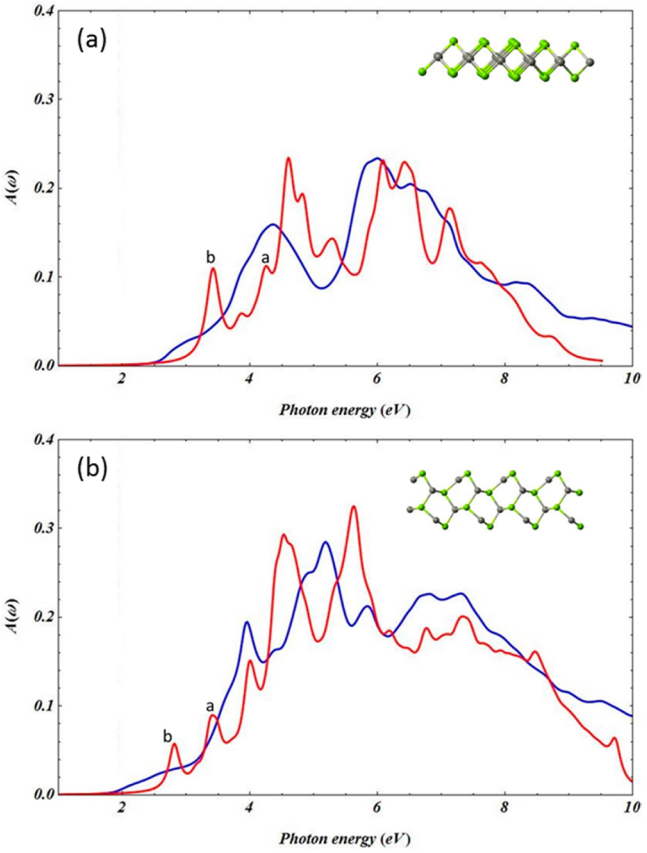

Figure 5. Optical absorbance spectra $A(\omega)$ calculated by *GW*_BSE (red) and RPA (blue) both using CSHIFT=0.1 for the ultrathin single-layer ZnSe (a) and the ZB110 double-layer ZnSe from ref 2 (b). Peaks with labels a and b correspond to the direct quasiparticle band gaps obtained by the G_0W_0 approach and to the exciton formations, respectively.

ZB100 single-layer sheet and the experimentally realized ZB110 double-layer sheet of ZnSe. For both of these 2D sheets, the BSE results evidenced the existence of a strong excitonic effect. As can be seen from each of the BSE spectra, peak a corresponds to the direct quasiparticle band gap obtained by the G_0W_0 approach, which is 4.21 and 3.37 eV for the ZB100 single-layer ZnSe and the ZB110 double-layer ZnSe, respectively. Thus, the energy difference between the band gap and peak b associated with the exciton formation provides an exciton binding energy of 0.79 and 0.55 eV for the ZB100 single-layer ZnSe and the ZB110 double-layer ZnSe, respectively. It is interesting that the photoelectrochemical test using the freestanding 2D ZB110 double-layer ZnSe sheet for solar water splitting exhibits a photocurrent density 4−10 times higher than that of ligand-coated colloidal layers, 8 times

DOI: 10.1021/am505655m
ACS Appl. Mater. Interfaces 2015, 7, 1458−1464

higher than quantum dots, and nearly 200 times higher than that of its 3D bulk.[2] The incident photon-to-current conversion efficiency (IPCE) of 42.5% at 300 nm for the freestanding ZB110 double-layer sheet is also strikingly higher than that of the rest of the materials studied.[2] The high photocurrent density and IPCE of the freestanding ZB110 double-layer sheet may have benefited from its strong optical absorbance (Figure 5b). Comparing the ultrathin ZB100 single-layer sheet with the ZB110 double-layer sheet, the largest absorption of the former occurs at a similar wavelength, suggesting a comparable performance on IPCE for applications targeting solar water splitting, among other potential applications.

CONCLUSIONS

In summary, we have discovered a novel ultrathin single-layer ZnSe through ab initio MD simulations, and investigated its electronic and optical properties by DFT and state-of-the-art many-body perturbation theory. The 3.0 Å thick single-layer ZnSe sheet consists of a square lattice of alternating Zn and Se atoms, resembling a single layer of atoms excised out of the bulk rocksalt structure of ZnSe but with a strong corrugation due to the tetrahedral and pyramidal coordinations of Zn and Se. Phonon dispersions without any imaginary frequencies provided evidence that the new single-layer ZnSe is dynamically stable, allowing its freestanding layer to be synthesized. Interestingly, this novel ultrathin single-layer sheet demonstrates a quantum confinement effect stronger than that of the experimentally realized double-layer honeycomb sheet of ZnSe with a thickness of 6.5 Å. The direct band gap at the Γ point is 4.21 eV according to the quasiparticle G_0W_0 calculation, showing a stronger enhancement than the double-layer honeycomb sheet relative to that of the ZB bulk phase of ZnSe. A strong excitonic effect has been revealed by BSE calculations. The exciton has a binding energy of 0.79 eV. According to the BSE calculations, the largest optical absorption of the ultrathin single-layer ZnSe occurs at a similar wavelength to the double-layer honeycomb sheet of ZnSe. Intriguingly, the ultrathin single-layer ZnSe found is very similar to the square lattice structure of the layered sheets in tetragonal tin monoxide SnO.[44] Recently, free-floating few-layer sheets of SnO have been fabricated through a liquid exfoliation and layer-by-layer assembly strategies, which also show high IPCE for solar water splitting.[45] Similar to the experimentally synthesized few-layer SnO and double-layer ZnSe, we envision that an ultrathin single-layer sheet of ZnSe with a square lattice can be synthesized. One straightforward way would be to exfoliate the ultrathin single-layer ZB100 sheet out of the PbO-type tetragonal structure of ZnSe proposed theoretically,[46] should it be synthesized in the future. Conversely, following the layer-by-layer assembly strategy demonstrated for SnO, the single-layer sheets of ZnSe, if made from the zinc blende phase, may be stacked together giving few-layer ZnSe sheets, which may enable thickness-dependent band gaps to be engineered. These freestanding sheets will likely show superior behavior on incident photon-to-current conversion efficiency for solar water splitting, among a wealth of potential applications.

ASSOCIATED CONTENT

Supporting Information

Computational details; additional ab initio MD simulation results; lattice vectors and Cartesian coordinates of the three-atom-thick ZnSe sheet; absorbance coefficient $\alpha(\omega)$ of the ZB bulk ZnSe. This material is available free of charge via the Internet at http://pubs.acs.org.

AUTHOR INFORMATION

Corresponding Author

*J. Zhou. Phone +1-865-574-7192. E-mail: jiajoe@gmail.com.

Notes

The authors declare no competing financial interest.

ACKNOWLEDGMENTS

We thank Drs. Yu Xie and Houlong Zhuang for helpful discussions. We are also indebted to Prof. Georg Kresse for kindly providing the latest PAW potentials with norm-conserving partial waves for Zn and Se. This work was supported by the Center for Nanophase Materials Sciences, which is sponsored at ORNL by the Scientific User Facilities Division, Office of Basic Energy Sciences, U.S. Department of Energy. This work used computational resources of the Oak Ridge Leadership Computing Facility at Oak Ridge National laboratory and of the National Energy Research Scientific Computing Center, which are supported by the Office of Science of the U.S. Department of Energy under Contract Nos. DE-AC05-00OR22750 and DE-AC02-05CH11231, respectively.

REFERENCES

(1) Ithurria, S.; Tessier, M. D.; Mahler, B.; Lobo, R. P. S. M.; Dubertret, B.; Efros, A. L. Colloidal Nanoplatelets with Two-Dimensional Electronic Structure. *Nat. Mater.* **2011**, *10*, 936−941.

(2) Sun, Y.; Sun, Z.; Gao, S.; Cheng, H.; Liu, Q.; Piao, J.; Yao, T.; Wu, C.; Hu, S.; Wei, S.; Xie, Y. Fabrication of Flexible and Freestanding Zinc Chalcogenide Single Layers. *Nat. Commun.* **2012**, *3*, 1057.

(3) Ithurria, S.; Dubertret, B. Quasi 2D Colloidal CdSe Platelets with Thicknesses Controlled at the Atomic Level. *J. Am. Chem. Soc.* **2008**, *130*, 16504−16505.

(4) Son, J. S.; Wen, X.-D.; Joo, J.; Chae, J.; Baek, S.-i.; Park, K.; Kim, J. H.; An, K.; Yu, J. H.; Kwon, S. G.; Choi, S. H.; Wang, Z. W.; Kim, Y. W.; Kuk, Y.; Hoffmann, R.; Hyeon, T. Large-Scale Soft Colloidal Template Synthesis of 1.4 nm Thick CdSe Nanosheets. *Angew. Chem., Int. Ed.* **2009**, *48*, 6861−6864.

(5) Ithurria, S.; Bousquet, G.; Dubertret, B. Continuous Transition from 3D to 1D Confinement Observed during the Formation of CdSe Nanoplatelets. *J. Am. Chem. Soc.* **2011**, *133*, 3070−3077.

(6) Li, Z.; Peng, X. Size/Shape-Controlled Synthesis of Colloidal CdSe Quantum Disks: Ligand and Temperature Effects. *J. Am. Chem. Soc.* **2011**, *133*, 6578−6586.

(7) Peng, Z. A.; Peng, X. Formation of High-Quality CdTe, CdSe, and CdS Nanocrystals Using CdO as Precursor. *J. Am. Chem. Soc.* **2000**, *123*, 183−184.

(8) Barrelet, C. J.; Wu, Y.; Bell, D. C.; Lieber, C. M. Synthesis of CdS and ZnS Nanowires Using Single-Source Molecular Precursors. *J. Am. Chem. Soc.* **2003**, *125*, 11498−11499.

(9) Huang, X.; Li, J. From Single to Multiple Atomic Layers: A Unique Approach to the Systematic Tuning of Structures and Properties of Inorganic−Organic Hybrid Nanostructured Semiconductors. *J. Am. Chem. Soc.* **2007**, *129*, 3157−3162.

(10) Novoselov, K. S.; Geim, A. K.; Morozov, S. V.; Jiang, D.; Zhang, Y.; Dubonos, S. V.; Grigorieva, I. V.; Firsov, A. A. Electric Field Effect in Atomically Thin Carbon Films. *Science* **2004**, *306*, 666−669.

(11) Novoselov, K. S.; Geim, A. K.; Morozov, S. V.; Jiang, D.; Katsnelson, M. I.; Grigorieva, I. V.; Dubonos, S. V.; Firsov, A. A. Two-Dimensional Gas of Massless Dirac Fermions in Graphene. *Nature* **2005**, *438*, 197−200.

(12) Butler, S. Z.; Hollen, S. M.; Cao, L.; Cui, Y.; Gupta, J. A.; Gutiérrez, H. R.; Heinz, T. F.; Hong, S. S.; Huang, J.; Ismach, A. F.;

DOI: 10.1021/am505655m
ACS Appl. Mater. Interfaces 2015, 7, 1458−1464

Johnston-Halperin, E.; Kuno, M.; Plashnitsa, V. V.; Robinson, R. D.; Ruoff, R. S.; Salahuddin, S.; Shan, J.; Shi, L.; Spencer, M. G.; Terrones, M.; Windl, W.; Goldberger, J. E. Progress, Challenges, and Opportunities in Two-Dimensional Materials Beyond Graphene. *ACS Nano* **2013**, *7*, 2898−2926.
(13) Rao, C. N. R.; Ramakrishna Matte, H. S. S.; Maitra, U. Graphene Analogues of Inorganic Layered Materials. *Angew. Chem., Int. Ed.* **2013**, *52*, 13162−13185.
(14) Tang, Q.; Zhou, Z. Graphene-Analogous Low-Dimensional Materials. *Prog. Mater. Sci.* **2013**, *58*, 1244−1315.
(15) Zhou, J.; Huang, J.; Sumpter, B. G.; Kent, P. R. C.; Terrones, H.; Smith, S. C. Structures, Energetics, and Electronic Properties of Layered Materials and Nanotubes of Cadmium Chalcogenides. *J. Phys. Chem. C* **2013**, *117*, 25817−25825.
(16) Zhou, J.; Huang, J.; Sumpter, B. G.; Kent, P. R. C.; Xie, Y.; Terrones, H.; Smith, S. C. Theoretical Predictions of Freestanding Honeycomb Sheets of Cadmium Chalcogenides. *J. Phys. Chem. C* **2014**, *118*, 16236−16245.
(17) Wen, X.-D.; Hoffmann, R.; Ashcroft, N. W. Two-Dimensional CdSe Nanosheets and Their Interaction with Stabilizing Ligands. *Adv. Mater. (Weinheim, Ger.)* **2013**, *25*, 261−266.
(18) Miro, P.; Audiffred, M.; Heine, T. An Atlas of Two-Dimensional Materials. *Chem. Soc. Rev.* **2014**, *43*, 6537−6554.
(19) Huang, X.; Li, J.; Fu, H. The First Covalent Organic−Inorganic Networks of Hybrid Chalcogenides: Structures That May Lead to a New Type of Quantum Wells. *J. Am. Chem. Soc.* **2000**, *122*, 8789−8790.
(20) Huang, X.; Li, J.; Zhang, Y.; Mascarenhas, A. From 1D Chain to 3D Network: Tuning Hybrid II-VI Nanostructures and Their Optical Properties. *J. Am. Chem. Soc.* **2003**, *125*, 7049−7055.
(21) Kresse, G.; Hafner, J. Ab Initio Molecular Dynamics for Liquid Metals. *Phys. Rev. B* **1993**, *47*, 558−561.
(22) Kresse, G.; Hafner, J. Ab Initio Molecular-Dynamics Simulation of the Liquid-Metal−Amorphous-Semiconductor Transition in Germanium. *Phys. Rev. B* **1994**, *49*, 14251−14269.
(23) Kresse, G.; Furthmüller, J. Efficiency of Ab-Initio Total Energy Calculations for Metals and Semiconductors Using a Plane-Wave Basis Set. *Comput. Mater. Sci.* **1996**, *6*, 15−50.
(24) Kresse, G.; Furthmüller, J. Efficient Iterative Schemes for Ab Initio Total-Energy Calculations Using a Plane-Wave Basis Set. *Phys. Rev. B* **1996**, *54*, 11169−11186.
(25) Blöchl, P. E. Projector Augmented-Wave Method. *Phys. Rev. B* **1994**, *50*, 17953−17979.
(26) Kresse, G.; Joubert, D. From Ultrasoft Pseudopotentials to the Projector Augmented-Wave Method. *Phys. Rev. B* **1999**, *59*, 1758−1775.
(27) Perdew, J. P.; Burke, K.; Ernzerhof, M. Generalized Gradient Approximation Made Simple. *Phys. Rev. Lett.* **1996**, *77*, 3865−3868.
(28) Perdew, J. P.; Burke, K.; Ernzerhof, M. Generalized Gradient Approximation Made Simple [Phys. Rev. Lett. 77, 3865 (1996)]. *Phys. Rev. Lett.* **1997**, *78*, 1396−1396.
(29) Rabadanov, M. K.; Loshmanov, A. A.; Shaldin, Y. V. Anharmonic Thermal Vibrations of Atoms in Crystals with Sphalerite Structure - GaP, ZnS, ZnSe, and ZnTe: High-Temperature X-ray Structure Studies. *Crystallogr. Rep.* **1997**, *42*, 592−602.
(30) Grimme, S. Semiempirical GGA-Type Density Functional Constructed with a Long-Range Dispersion Correction. *J. Comput. Chem.* **2006**, *27*, 1787−1799.
(31) Rödl, C.; Bechstedt, F. Optical and Energy-Loss Spectra of the Antiferromagnetic Transition Metal Oxides MnO, FeO, CoO, and NiO Including Quasiparticle and Excitonic Effects. *Phys. Rev. B* **2012**, *86*, 235122.
(32) Rinke, P.; Schleife, A.; Kioupakis, E.; Janotti, A.; Rödl, C.; Bechstedt, F.; Scheffler, M.; Van de Walle, C. G. First-Principles Optical Spectra for F Centers in MgO. *Phys. Rev. Lett.* **2012**, *108*, 126404.
(33) Giannozzi, P.; Baroni, S.; Bonini, N.; Calandra, M.; Car, R.; Cavazzoni, C.; Ceresoli, D.; Chiarotti, G. L.; Cococcioni, M.; Dabo, I.; Dal Corso, A.; de Gironcoli, S.; Fabris, S.; Fratesi, G.; Gebauer, R.; Gerstmann, U.; Gougoussis, C.; Kokalj, A.; Lazzeri, M.; Martin-Samos, L.; Marzari, N.; Mauri, F.; Mazzarello, R.; Paolini, S.; Pasquarello, A.; Paulatto, L.; Sbraccia, C.; Scandolo, S.; Sclauzero, G.; Seitsonen, A. P.; Smogunov, A.; Umari, P.; Wentzcovitch, R. M. QUANTUM ESPRESSO: A Modular and Open-Source Software Project for Quantum Simulations of Materials. *J. Phys.: Condens. Matter* **2009**, *21*, 395502.
(34) Gangadharan, R.; Jayalakshmi, V.; Kalaiselvi, J.; Mohan, S.; Murugan, R.; Palanivel, B. Electronic and Structural Properties of Zinc Chalcogenides ZnX (X=S, Se, Te). *J. Alloys Compd.* **2003**, *359*, 22−26.
(35) Mujica, A.; Rubio, A.; Muñoz, A.; Needs, R. J. High-Pressure Phases of Group-IV, III−V, and II−VI Compounds. *Rev. Mod. Phys.* **2003**, *75*, 863−912.
(36) Tusche, C.; Meyerheim, H. L.; Kirschner, J. Observation of Depolarized ZnO(0001) Monolayers: Formation of Unreconstructed Planar Sheets. *Phys. Rev. Lett.* **2007**, *99*, 026102.
(37) Weirum, G.; Barcaro, G.; Fortunelli, A.; Weber, F.; Schennach, R.; Surnev, S.; Netzer, F. P. Growth and Surface Structure of Zinc Oxide Layers on a Pd(111) Surface. *J. Phys. Chem. C* **2010**, *114*, 15432−15439.
(38) Karazhanov, S. Z.; Ravindran, P.; Kjekshus, A.; Fjellvåg, H.; Svensson, B. G. Electronic Structure and Optical Properties of ZnX (X=O, S, Se, Te): A Density Functional Study. *Phys. Rev. B* **2007**, *75*, 155104.
(39) Datta, S.; Saha-Dasgupta, T.; Sarma, D. D. Wannier Function Study of the Relative Stability of Zinc-Blende and Wurtzite Structures in the CdX (X = S, Se, Te) Series. *J. Phys.: Condens. Matter* **2008**, *20*, 445217.
(40) Perdew, J. P. Density Functional Theory and the Band Gap Problem. *Int. J. Quantum Chem.* **1985**, *28*, 497−523.
(41) Grüneis, A.; Kresse, G.; Hinuma, Y.; Oba, F. Ionization Potentials of Solids: The Importance of Vertex Corrections. *Phys. Rev. Lett.* **2014**, *112*, 096401.
(42) Klimeš, J.; Kaltak, M.; Kresse, G. Predictive GW Calculations Using Plane Waves and Pseudopotentials. *Phys. Rev. B* **2014**, *90*, 075125.
(43) Yang, L.; Deslippe, J.; Park, C.-H.; Cohen, M. L.; Louie, S. G. Excitonic Effects on the Optical Response of Graphene and Bilayer Graphene. *Phys. Rev. Lett.* **2009**, *103*, 186802.
(44) Wells, A. F. *Structural Inorganic Chemistry*; 5th ed.; Clarendon: Oxford, U. K., 1984.
(45) Liang, L.; Sun, Y.; Lei, F.; Gao, S.; Xie, Y. Free-Floating Ultrathin Tin Monoxide Sheets for Solar-Driven Photoelectrochemical Water Splitting. *J. Mater. Chem. A* **2014**, *2*, 10647−10653.
(46) Ding, Y.; Wang, Y.; Ni, J. Electronic and Magnetic Properties of 3d Transition-Metal Selenides from First Principles. *Solid State Commun.* **2009**, *149*, 505−509.

DOI: 10.1021/am505655m
ACS Appl. Mater. Interfaces 2015, 7, 1458−1464